

Magnetostatic Boson Stars

Víctor Jaramillo and Darío Núñez

*Instituto de Ciencias Nucleares, Universidad Nacional Autónoma de México,
Circuito Exterior C.U., A.P. 70-543, México D.F. 04510, México*

(Dated: September 19, 2022)

We solve the Einstein-Maxwell-Klein-Gordon system of equations and derive a compact, static axially symmetric magnetized object which is electrically neutral and made of two complex massive charged scalar fields. We describe several properties of such solution, including the torus form of the matter density and the expected dipolar distribution of the magnetic field, with some peculiar features in the central regions. The solution shows no divergencies in any of the field and metric functions. A discussion is presented on a case where the gravitational and magnetic fields in the external region are similar to those of neutron stars.

PACS numbers: 04.20.-q, 04.25.Dm, 95.30.Sf

I. INTRODUCTION

Boson stars are self-gravitating solitons made up of complex scalar field. These objects are interesting for various reasons. They serve as simple models for compact objects in the interplay of Field Theory and General Relativity and are also interesting on their own since they possess important dynamical properties that allow to study them in hypothetical strong gravity astrophysical scenarios, for example, in the gravitational waveform research; see *e.g.* [1]. Bosonic stars have applications also as black hole mimickers [2, 3] and, more generally, scalar fields are relevant in cosmology as quintessence [4], ultralight dark matter [5–7] and as a source of inflation [8].

Static and stationary single field configurations have been presented in the literature in the past years (for reviews see Refs. [9–11]), for instance, the free and massive bosonic field solution of the Einstein-Klein-Gordon equations in spherical symmetry [12] can be generalized gauging the global $U(1)$ symmetry, which leads to the charged version of boson stars [13]. Rotating generalizations of boson stars were obtained in [14] within the Einstein-Klein-Gordon setup and in the Einstein-Klein-Gordon-Maxwell extension, the charged rotating one [15]. In these models the coupling constant parameter is freely specifiable, however, in order to obtain equilibrium solutions, the value of the coupling parameter ranges from zero up to a critical value [13, 15].

Staying within the complex, massive, free scalar field case there are two more characterizations that can be found in the literature up to the present time, these are the multipolar boson stars [16], which are static nonspherical configurations with similar morphologies to the probability density of atomic orbitals and the multi-field (ℓ -) boson stars [17–19], in which the $U(1)$ symmetry is generalized by considering a $U(N)$ symmetry. Of particular interest in this paper is the toroidal static boson star of [19], which can be understood as the superposition of two contrarotating solutions that give rise to a static equilibrium configuration.

The rotating charged boson stars share some properties with the uncharged rotating case, such as the toroidal shape and with the charged (electrostatic) case, such as the critical value of the coupling constant. As one would expect the charged and rotating general solutions include electric charge and magnetic dipole moment with the particularity that the magnetic moment is nonzero only if the electric charge is nonzero, therefore obtaining solutions where both electric and magnetic fields are present in the local inertial frame of zero angular momentum. Until now, no electrically neutral and magnetized self-gravitating bosonic stars have been constructed, which might be relevant models in the study of strong gravity and magnetic fields phenomena.

Magnetic fields play an important role in many astrophysical scenarios. Some of the relativistic applications involve compact, electrically neutral objects and strong magnetic fields where their self-gravitation must be taken into account. Fully relativistic and self-consistent models of neutron stars with magnetic fields were first presented in [20] (see also *e.g.* [21, 22] for poloidal and [23–25] for toroidal magnetic fields). These are numerical solutions of the Einstein-Maxwell-Euler system in axial symmetry which can possess angular momentum and total electric charge. Even the globally neutral and static cases are deformed by the effect of the magnetic field, changing in consequence the global properties of the equilibrium configurations.

The purpose of this paper is to construct and study magnetostatic solutions of boson stars with zero total electric charge. To do so we obtain a generalization of the toroidal static boson stars by coupling the scalar fields to the electromagnetic field, we shall show that the gauge coupling parameter can exceed the critical value obtained for the electrostatic boson stars. In Sec. II we present the action for the model, the ansätze for the fields and the conserved quantities. Then, in Sec. III we describe the numerical procedure and the construct sequence of solutions with different values of the coupling parameter, discussing the physical properties of the configurations. The magnetic field for the constructed solutions and a comparison with strongly magnetized neutron stars is presented Sec. IV. We conclude our manuscript and give some perspectives of future works in Sec. V. In Appendix A we give the complete set of elliptic partial differential equations of our model together with explicit expressions for the $3+1$ decomposition of the energy momentum tensor. We work with $c = G = 1$ and the metric signature is taken to be $(-, +, +, +)$.

II. MODEL

A single electrically charged scalar field in spherical symmetry allows to construct charged boson stars, which are static solutions that give rise to an electric field as measured by an observer at rest [13]. Even the rotating generalization of this configurations, which also generate a magnetic field, possess an electric field that does not vanish [15]. There are no immediate simple models consisting of one scalar field that give rise to magnetostatic self-gravitating solutions, however the multifield approach leads to a natural way of obtaining such boson stars.

On the other hand, although fully relativistic neutron stars with magnetic fields have been constructed, all the solutions (to the best of our knowledge) have been obtained using the free current assumption, i.e., electromagnetic sources J^μ independent to the fluid movement. This means in particular that in the (magneto)static solutions the fluid is at rest while the spatial components of the electric current are nonzero. This is a limiting assumption, and as pointed out in [22], in principle the currents should be derived from a microscopic model which “would require a multifluid approach to model the movements of free protons and electrons”.

For boson stars, in the Einstein-Klein-Gordon-Maxwell framework, the free current assumption cannot be even made since the electric current is determined by the scalar fields, however the multifield approach is feasible. In our approach globally neutral configurations are constructed by superposition of two contrarotating “thick current loops” made of charged scalar fields.

The general framework in which magnetized boson stars are constructed consists of two self-gravitating complex scalar fields minimally coupled to the electromagnetic four-potential with coupling constants of opposite sign. In this section we summarize the basic equations needed to construct the solutions and the conserved quantities that will be useful in the analysis.

A. Field equations

We consider two massive complex scalar fields, $\Phi_{(1)}$ and $\Phi_{(2)}$, minimally coupled to the Einsteinian gravity and to the electromagnetic field,

$$S = \int d^4x \sqrt{-g} \left[\frac{1}{16\pi} R - \frac{1}{2} \sum_{j=1}^2 \left(g^{\mu\nu} (D_\mu^{(j)} \Phi_{(j)}) (D_\nu^{(j)} \Phi_{(j)})^* + \mu^2 |\Phi_{(j)}|^2 \right) - \frac{1}{4\mu_0} F_{\mu\nu} F^{\mu\nu} \right], \quad (1)$$

where $F_{\mu\nu} = \partial_\mu A_\nu - \partial_\nu A_\mu$ is the Faraday tensor and the covariant derivative operators, $D_\mu^{(1)} = \nabla_\mu + iqA_\mu$ and $D_\mu^{(2)} = \nabla_\mu - iqA_\mu$ couple both scalar fields with A_μ . Notice that we have chosen equal mass terms for both scalar fields and opposite signs for the electromagnetic coupling constants (boson charges). The scalar fields interact with each other indirectly, through gravity and the electromagnetic field.

Variation of Eq. (1), with respect to the different fields leads to the Euler-Lagrange equations of the model (see *e.g.* [26]). Variation with respect to $g_{\mu\nu}$ leads to

$$R_{\mu\nu} - \frac{1}{2} R g_{\mu\nu} = 8\pi T_{\mu\nu}; \quad (2a)$$

$$T_{\mu\nu} = T_{\mu\nu}^{(1)} + T_{\mu\nu}^{(2)} + (T^{\text{EM}})_{\mu\nu}, \quad (2b)$$

$$T_{\mu\nu}^{(j)} := \frac{1}{2} (D_\mu^{(j)} \Phi_{(j)}) (D_\nu^{(j)} \Phi_{(j)})^* + \frac{1}{2} (D_\nu^{(j)} \Phi_{(j)}) (D_\mu^{(j)} \Phi_{(j)})^* - \frac{1}{2} g_{\mu\nu} \left(g^{\alpha\beta} (D_\alpha^{(j)} \Phi_{(j)}) (D_\beta^{(j)} \Phi_{(j)})^* + \mu^2 |\Phi_{(j)}|^2 \right), \quad (2c)$$

$$(T^{\text{EM}})_{\mu\nu} := \frac{1}{\mu_0} F_{\mu\sigma} F_{\nu\lambda} g^{\sigma\lambda} - \frac{1}{4\mu_0} g_{\mu\nu} F_{\alpha\beta} F^{\alpha\beta}. \quad (2d)$$

The equation for the fields $\Phi_{(1)}$ and $\Phi_{(2)}$ are the Klein-Gordon equations,

$$g^{\mu\nu} D_\nu^{(j)} D_\mu^{(j)} \Phi_{(j)} = \mu^2 \Phi_{(j)}. \quad (3)$$

Variation with respect to A_μ leads to the Maxwell equations with source the charged scalar fields which define a current four-vector J^μ ,

$$\nabla_\nu F^{\mu\nu} = \mu_0 J^\mu := \mu_0 (q j_1^\mu - q j_2^\mu); \quad (4a)$$

$$j_i^\mu := \frac{i g^{\mu\nu}}{2} (\Phi_{(i)}^* D_\nu^{(i)} \Phi_{(i)} - \Phi_{(i)} (D_\nu^{(i)} \Phi_{(i)})^*), \quad (4b)$$

here J^μ is the (total) electromagnetic current.

B. Global quantities

The spacetime we will consider in this work is stationary (static) and axisymmetric. Komar expressions allow to calculate global quantities for each of this isometries; if ξ is the Killing vector associated with stationarity, Σ_t is a spacelike surface and n^μ the unit vector normal to this hypersurface, then the quantity,

$$M = \frac{1}{4\pi} \int_{\Sigma_t} R_{\mu\nu} n^\mu \xi^\nu dV, \quad (5)$$

defines the Komar mass. Similarly, if χ is the Killing vector associated with the axial symmetry, the quantity

$$J = \frac{1}{8\pi} \int_{\Sigma_t} R_{\mu\nu} n^\mu \chi^\nu. \quad (6)$$

gives the angular momentum of the spacetime.

The quantities j_1^μ and j_2^μ defined in Eq. (4) are Noether density currents ($\nabla_\mu j^\mu = 0$) which arise from the invariance of Eq. (1) under the $U(1)$ gauge transformation of $\Phi_{(1)}$ and $\Phi_{(2)}$. It follows that integration of the projection onto n^μ of this currents over Σ_t leads to the conserved particle numbers

$$\mathcal{N}_1 = \int_{\Sigma_t} j_1^\mu n_\mu dV, \quad \mathcal{N}_2 = \int_{\Sigma_t} j_2^\mu n_\mu dV; \quad \mathcal{N} := \mathcal{N}_1 + \mathcal{N}_2. \quad (7)$$

In the rotating boson stars, it was shown [14, 27, 28] that the angular momentum J takes values that are integer multiples of the particle number, $J = m\mathcal{N}$, with m the winding number (defined below) of the scalar field ansatz, this result is also valid in the charged rotating case [15]. However, in the magnetized solutions obtained in this work this relation does not hold since they are by construction $J = 0$ static, as will be argued in the next section.

The associated total electric charge, related to the sources at the Maxwell equation is given by $Q = \int_{\Sigma_t} J^\mu n_\mu dV = q(\mathcal{N}_1 - \mathcal{N}_2)$. In the single field static and rotating charged boson stars the total charge of the system is related to the particle number by $Q = q\mathcal{N}$ and it was obtained [13] that Q coincides with the asymptotic value extracted from the electric potential and matches the exterior Reissner-Nordström solution. Again, the relation $Q = q\mathcal{N}$ is not valid for our case because, as we will see bellow, the obtained solutions satisfy $Q = 0$.

C. Static axisymmetric spacetime and Ansätze for the fields

In coordinates adapted to the Killing fields, where $\xi = \partial/\partial t$ and $\chi = \partial/\partial\varphi$, the static and axially symmetric line element we will consider is in the Lewis-Papetrou form,

$$g_{\mu\nu} dx^\mu dx^\nu = -e^{2F_0} dt^2 + e^{2F_1} (dr^2 + r^2 d\theta^2) + e^{2F_2} r^2 \sin^2 \theta d\varphi^2, \quad (8)$$

where the metric functions F_0 , F_1 and F_2 depend only on the coordinates r and θ . We have used the same line element as the one in Ref. [19], where the toroidal static boson star is constructed, however, the $g_{t\varphi}$ term usually written as the function $w(r, \theta)$ or $w(r, \theta)/r$, is not included in (8) because we are looking for static configurations with zero total angular momentum J , and in this case it can be seen [29, 30] that $w = 0$ if and only if the spacetime is static.

The contribution of the scalar fields in the energy-momentum tensor, $T_{\mu\nu}^{(1)}$, $T_{\mu\nu}^{(2)}$ will be consistently independent of t and φ if for the scalar fields we use the following ansatz, which is similar to the one used for rotating, multifield, multifrequency boson stars and even for chains [31],

$$\Phi_{(1)} = \phi(r, \theta) e^{i\omega t - im\varphi}; \quad \Phi_{(2)} = \phi(r, \theta) e^{i\omega t + im\varphi}. \quad (9)$$

Here m is an integer called winding number. Moreover, the opposite sign of this parameter for each field in Eq. (9) can be interpreted as having contra-rotating scalar fields distributions. It is not difficult to obtain that with this election of winding numbers, $T_{t\varphi}^{(1)} = -T_{t\varphi}^{(2)}$, consistent with the Einstein tensor component $G_{t\varphi}$ being zero for the metric in Eq. (8).

Again, analyzing the components of the Einstein tensor we can elucidate the ansatz for the field A_μ . Two possibilities for the electromagnetic four-potential are compatible with the spacetime at hand: the purely poloidal ($A_r = A_\theta = 0$) and the purely toroidal ($A_t = A_\varphi = 0$) magnetic fields [23, 24], however only the first possibility can be realized given the ansatz (9) chosen for the scalar fields since only the J^φ source of the Maxwell equations is nonzero¹, which additionally implies that $A_t = \text{constant}$, therefore we adopt

$$A_\mu dx^\mu = C(r, \theta) d\varphi. \quad (10)$$

The resulting number density currents, given in Eqs. (A11) and (A11), imply $Q = 0$ since $J^\mu n_\mu = 0$.

¹ In the single field charged rotating star, also the J^t component is nonzero, in our case however $j_1^t = j_2^t$, see Appendix A.

III. NUMERICAL SOLUTIONS

A. Boundary Conditions and numerical method

In order to construct magnetostatic solutions of boson stars, the Einstein-Klein-Gordon-Maxwell system is solved. This means solving for the five functions $\{\phi, C, F_0, F_1, F_2\}$ and the unknown parameter ω , imposing the appropriate symmetries and boundary conditions. The full elliptic system of coupled partial differential equations (PDEs) in r and θ is given in the Appendix A.

First, we impose even parity with respect to reflections at the equatorial plane of the five unknown functions which in particular implies that derivatives with respect to θ at $\theta = \pi/2$ vanish and also that the required integration domain reduces to $0 \leq \theta \leq \pi/2, 0 \leq r < \infty$.

Asymptotic flatness implies that the following outer boundary conditions must be imposed,

$$\begin{aligned} \phi|_{r \rightarrow \infty} &= 0, & C|_{r \rightarrow \infty} &= 0; \\ F_0|_{r \rightarrow \infty} &= 0, & F_1|_{r \rightarrow \infty} &= 0, & F_2|_{r \rightarrow \infty} &= 0. \end{aligned} \quad (11)$$

Also the condition $\omega < \mu$ is necessary in order to have $\phi|_{r \rightarrow \infty} = 0$. Regularity of the solution at the origin and on the symmetry axis require,

$$\begin{aligned} \phi|_{r=0} &= 0, & C|_{r=0} &= 0; \\ \partial_r F_0|_{r=0} &= 0, & \partial_r F_1|_{r=0} &= 0, & \partial_r F_2|_{r=0} &= 0, \\ F_1|_{r=0} &= F_2|_{r=0}. \end{aligned} \quad (12)$$

$$\begin{aligned} \phi|_{\theta=0,\pi} &= 0, & C|_{\theta=0,\pi} &= 0; \\ \partial_\theta F_0|_{\theta=0,\pi} &= 0, & \partial_\theta F_1|_{\theta=0,\pi} &= 0, & \partial_\theta F_2|_{\theta=0,\pi} &= 0, \\ F_1|_{\theta=0,\pi} &= F_2|_{\theta=0,\pi}. \end{aligned} \quad (13)$$

The regularity conditions for ϕ for the case $m = 0$ are different from those of the previous expressions, however this case reduce to the widely studied spherical, nonrotating, neutral boson star, and will not be addressed in this manuscript except for comparison.

The nonlinear PDEs are solved numerically using the spectral solver KADATH [32, 33] which implements a Newton-Raphson iteration. This library, which has been successfully applied to solve a wide variety of PDEs in theoretical physics and in particular in relativity, was also used in the construction of rotating boson stars [27].

Chebyshev polynomials have been used in the spectral method as basis functions for the expansions of the five unknown functions. The spatial domain is divided into 8 spherical shells with boundaries located at $r = \{2, 4, 8, 16, 32, 64, 128\}$. The regularity conditions in Eqs. (12) and (13) are either imposed by the spectral basis² for a given function on the corresponding domain, or checked that they hold up to numerical accuracy. On the other hand the outer boundary conditions in Eq. (11) are imposed “exactly” (without the need of a cutoff radius) given the compactification of the radial variable at the outermost spherical shell.

An initial guess for the functions is required in order to start the iteration. For each value of m this needs to be done only once. The expressions

$$N := e^{F_0} = 1 - (1 - N_0)e^{-r^2/r_0^2}, \quad F_1 = F_2 = 0, \quad C = 0, \quad (14)$$

also used in [35], and

$$\phi = \phi_0 (r \sin \theta)^m e^{-(x^2/2 + 2z^2)m/r_0^2} \quad (15)$$

with $x = r \sin \theta$, $z = r \cos \theta$, proposed in Ref. [27], have proven to be good guesses given certain choice of ϕ_0 , r_0 fixing the coupling constant $q = 0$ and the lapse at $r = 0$, $N_0 \approx 0.95$. The last condition prevents convergence to the trivial $\phi = 0$ solution and also leads to a Newtonian configuration ($\omega \sim \mu$). Once the first solution is obtained the rest of the solutions are obtained varying N_0 and increasing q by small steps.

In addition to the Komar expression on Eq. (5), the ADM mass definition can be used to obtain the total mass of the star. Both quantities should coincide given the stationarity of the spacetime we are considering [30], therefore the difference between the ADM and the Komar masses can be used as an indicator of the numerical accuracy and

² Details on how this is implemented in terms of the Chebyshev spectral basis in the innermost shell and on the symmetry axis for similar problems can be found in [27] and [34].

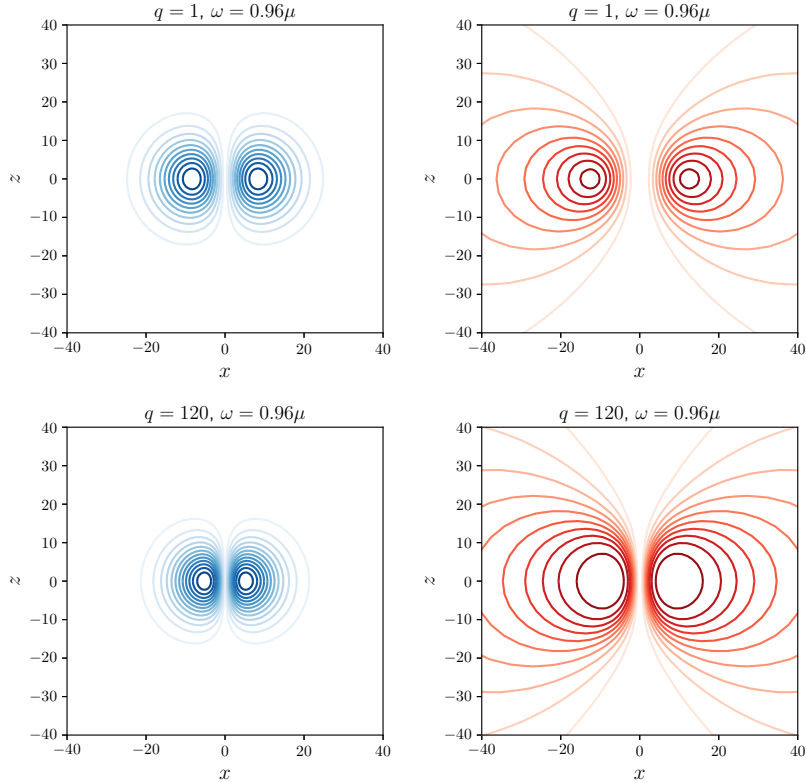


FIG. 1. Scalar field ϕ isocontours (left) and magnetic field lines (right) in a plane of constant φ with $x = r \sin \theta$ and $z = r \cos \theta$ for $m = 1$ and $\omega = 0.96\mu$ using different values of q .

provide an estimation of the numerical error of the solution. An expression for the ADM mass suitable for our case is the expression [30],

$$M = -\frac{1}{8\pi} \lim_{S \rightarrow \infty} \oint_S \left[\frac{\partial}{\partial r} (F_1 + F_2) + \frac{F_2 - F_1}{r} \right] r^2 \sin \theta d\theta d\varphi, \quad (16)$$

where the limit indicates integration over a sphere S of radius $r \rightarrow \infty$.

One can also verify that the value of the unknown frequency ω converge exponentially to a finite value with the number of collocation points. This error indicator has been used together with the relative difference of the ADM and Komar masses to monitor accuracy along the sequence of numerical solutions and to carry out convergence tests of the solutions with increasing number of spectral coefficients.

B. Structure of the stars

One can use the code to solve for boson stars of several types. The spectral code has been able to reproduce sequences of solutions already presented in the literature such as the single field static and the rotating mini-boson stars, as well as the multifield ℓ -boson stars and the toroidal static boson stars. In this section we present new solutions that correspond to magnetostatic boson stars. These configurations generalize the toroidal static boson stars, incorporating a new parameter, q , in addition to the frequency ω and the winding number m .

Typical solutions for magnetized ($q \neq 0$) boson stars are presented in Fig. 1, where isocontours of the scalar field function ϕ and the φ component of A_μ are plotted for $m = 1$. In the first place we can notice from the ϕ contours, that the star has a toroidal structure just like the $q = 0$ case, secondly we observe from the isocontours of C , which can be interpreted as the magnetic field lines (see Sec. IV), that the expected poloidal magnetic field distribution preserves as q increases, however, as we will show next in this paragraph, near to the location of maximum ϕ a region of constant C (zero magnetic field) is formed which grows in size. This effects on the structure of the star and the morphology of the magnetic field can be seen more clearly, plotting the profiles of the scalar field and the electromagnetic potential on the equatorial plane. This is done in Fig. 2 where we have plotted $m - qC$ instead of C , to observe an interesting property: Above certain value of q (which in the $\omega = 0.96\mu$ case of Fig. 2 is at $q \approx 50$, between the second and third panel), the quantity qC approaches but never exceeds m in a region that grows as q increases. In all of the solutions presented in this paper we have obtained $C(r) < m/q$ for all r .

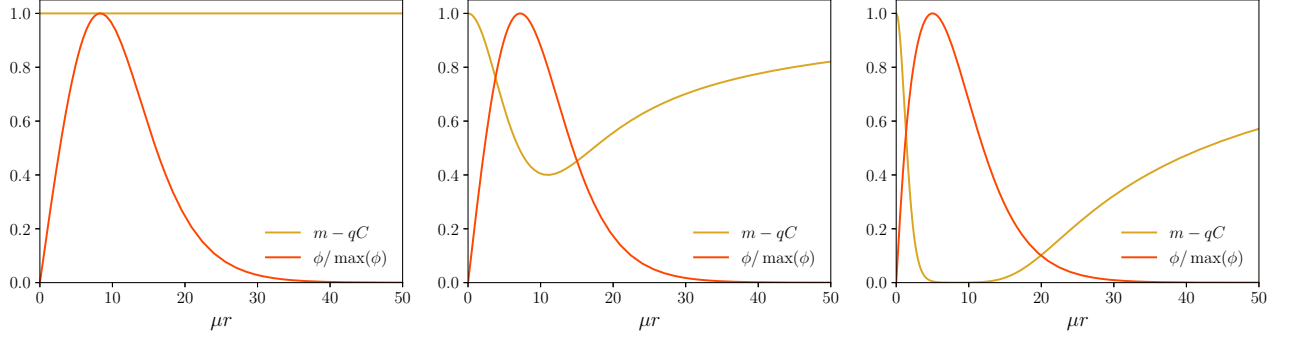


FIG. 2. Profiles of ϕ and C at the equatorial plane for solutions with $m = 1$ and $\omega = 0.96\mu$. Left panel: Neutral ($q = 0$). Center panel: $q = 25$. Right panel: $q = 140$.

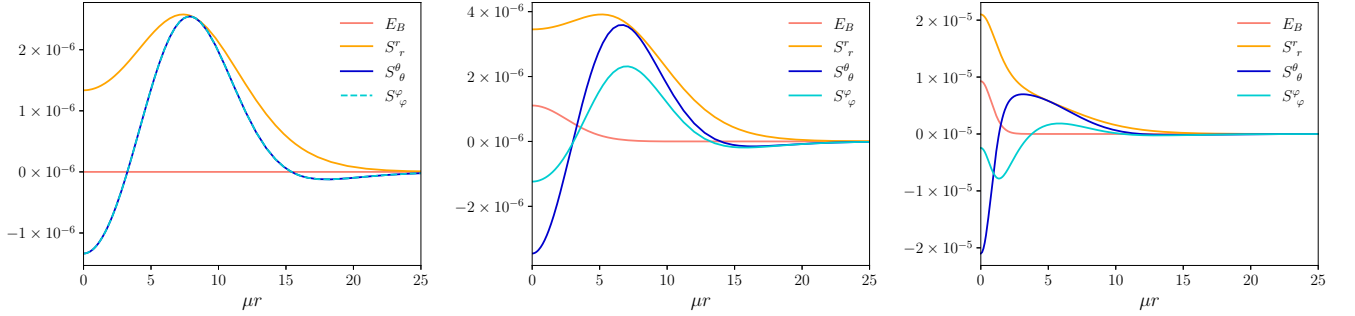


FIG. 3. Source terms at the equatorial plane for boson stars with $m = 1$ and $\omega = 0.96\mu$. Left panel: Neutral ($q = 0$). Center panel: $q = 25$. Right panel: $q = 140$.

The sources of gravitational field are also enlightening regarding the structure of the star as well as its global properties, as we will see in the next section. Restricting to the equatorial plane, $\theta = \pi/2$, the complete contributions of the energy momentum tensor (see Appendix. A) are given by,

$$E|_{\theta=\pi/2} = \left[\frac{\omega^2}{e^{2F_0}} + \frac{(k - qC)^2}{e^{2F_2}r^2} \right] \phi^2 + \frac{1}{e^{2F_1}} \left(\frac{\partial\phi}{\partial r} \right)^2 + \mu^2\phi^2 + E_B, \quad (17)$$

$$S^r_r|_{\theta=\pi/2} = \left[\frac{\omega^2}{e^{2F_0}} - \frac{(k - qC)^2}{e^{2F_2}r^2} \right] \phi^2 + \frac{1}{e^{2F_1}} \left(\frac{\partial\phi}{\partial r} \right)^2 - \mu^2\phi^2 + E_B, \quad (18)$$

$$S^\theta_\theta|_{\theta=\pi/2} = \left[\frac{\omega^2}{e^{2F_0}} - \frac{(k - qC)^2}{e^{2F_2}r^2} \right] \phi^2 - \frac{1}{e^{2F_1}} \left(\frac{\partial\phi}{\partial r} \right)^2 - \mu^2\phi^2 - E_B \quad (19)$$

$$S^\varphi_\varphi|_{\theta=\pi/2} = \left[\frac{\omega^2}{e^{2F_0}} + \frac{(k - qC)^2}{e^{2F_2}r^2} \right] \phi^2 - \frac{1}{e^{2F_1}} \left(\frac{\partial\phi}{\partial r} \right)^2 - \mu^2\phi^2 + E_B \quad (20)$$

Where we have defined E_B as the purely electromagnetic contribution to the energy density (at the equatorial plane),

$$E_B := \frac{1}{2r^2 e^{2F_1+2F_2}} \left(\frac{\partial C}{\partial r} \right)^2. \quad (21)$$

Regarding the stress tensor components, which are usually identified as components of the pressure, the system is completely anisotropic even in the $q = 0$ case, where for instance the difference $S^\theta_\theta - S^\varphi_\varphi \propto \phi^2 e^{-2F_2}/r^2$ is not zero, although suppressed by r^2 . In the left panel of Fig. 3 we plot the sources of the $q = 0$ case where in fact the difference between $S^\theta_\theta - S^\varphi_\varphi$ cannot be appreciated. The middle and right panels of Fig. 3 show the magnetized $q = 25$ and $q = 140$ cases respectively. Notice that the extrema of S^φ_φ decrease in magnitude with respect to the extrema of S^θ_θ and S^r_r . In particular near $r = 0$, the minimum of S^φ_φ increases due to the E_B contribution. The behavior of the pressure term S^φ_φ is relevant in the analysis of the effect of q on global quantities, as for example the magnetic dipole moment and the total mass. This will be discussed in the next section.

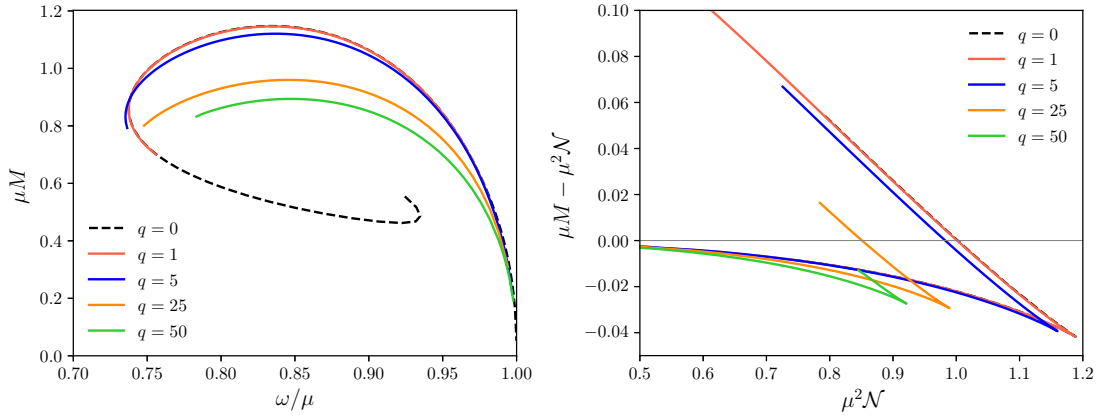


FIG. 4. Left panel: Frequency *vs.* mass for the $m = 1$ magnetostatic boson star solutions using different values of the coupling constant q . Right panel: Binding energy $M - \mu N$ for $m = 1$.

C. Sequence of magnetic boson stars

For $m = 1, 2$ we obtained a family of configurations by means of slowly varying the parameters of the solution starting from a Newtonian solution, as stated before. First, we have verified that in the case $q = 0$, $m = 1$ we obtain the known sequence of toroidal static boson stars [19]. Thereafter, starting from this set of solutions, we have slowly increased the value of q , generating in this way sequences of magnetized boson stars.

In Fig. 4, the global quantity M is shown *vs.* the scalar field frequency ω for $m = 1$ and five chosen values for q . Some interesting aspects arise from these solutions: firstly the mass of the star decreases monotonically with q ; this is the opposite behavior to that obtained in models of neutron stars with magnetic fields [20, 21], where their structure begins from spherical morphology at zero magnetic field (for the static case), and flattens, increasing the circumferential radius of the star, as the magnitude of the magnetic fields increase, with a corresponding increase in the mass of the star. The observed structure dependence on q of the magnetized boson stars, is also opposite to the corresponding dependence of charged boson stars as discussed in the previous section. However, such observed decrease on the size and total mass M as the coupling constant q grows, is also observed in the magnetized Bose-Einstein condensate stars [36].

The second aspect to consider about Fig. 4, regards the existence of equilibrium configurations with coupling constant q above the value $q_{\text{crit}} \approx 1/\sqrt{2}$. Indeed, as reported in [15, 37], that value was an upper limit for stable charged and stable rotating-charged boson stars. In our model without total charge, that limit is overcome. This interesting result is related to the fact that the Lorentz force,

$$f_\nu := F_{\nu\alpha} J^\alpha = -\nabla_\mu (T^{\text{EM}})^\mu_\nu, \quad (22)$$

points everywhere outwards for the charged mini-boson stars, while for the magnetostatic boson star it only points outward near the origin and points inward outside the main distribution of scalar field. Therefore, the nonrelativistic argument regarding Coulomb repulsion *vs.* gravitational attraction does not apply here. Instead, it is the stress anisotropy that ultimately determines the structure and global properties of the star, as we will see below in relation to the decrease in the total mass. Numerically we have not obtained any limiting value for the parameter q , the equations are difficult to solve for large values of the coupling constant due to the resolution required at the “edges of the plateau” that forms in the function C (see the right panel of Fig. 2).

Anisotropic pressures are essential to obtain equilibrium configurations with high compactness and large values for the mass. In [35] (see [38] for recent discussion on fluid anisotropic stars and [39] for shell-type configurations in the Einstein-Vlasov system) it was shown that for ℓ -boson stars, small radial pressures and big tangential pressures are related to an increase in the mass and radius of the star in a way that resembles the forces on an arch. In our case, to understand the decrease in size of the magnetic boson stars, we start by noticing that the tangential pressure is composed by two different contributions, S^θ_θ and S^φ_φ , which act together with the radial pressure (and with the Lorentz force in some region) against gravity in order to support the configuration. The toroidal shape, which is made possible by the S^φ_φ contribution, shrinks with increasing q - right panel Fig. 5, given that the electromagnetic contribution to the energy-momentum tensor in the region where the scalar field concentrates, is bigger for S^r_r than for the tangential components and in particular with respect to S^φ_φ , as discussed in Sec. III B. Our results indicate that this reduction in the size of the star is accompanied by a reduction in the total mass that the boson star can support.

Fig. 5 shows properties of the scalar field, ϕ and of the electromagnetic one, C *vs.* q . More precisely, the figure shows the maximum of the functions and the coordinate at which the maximum is attained. From the right panel we appreciate the decrease in size of the torus as a function of q for fixed ω . In the left panel we see another important

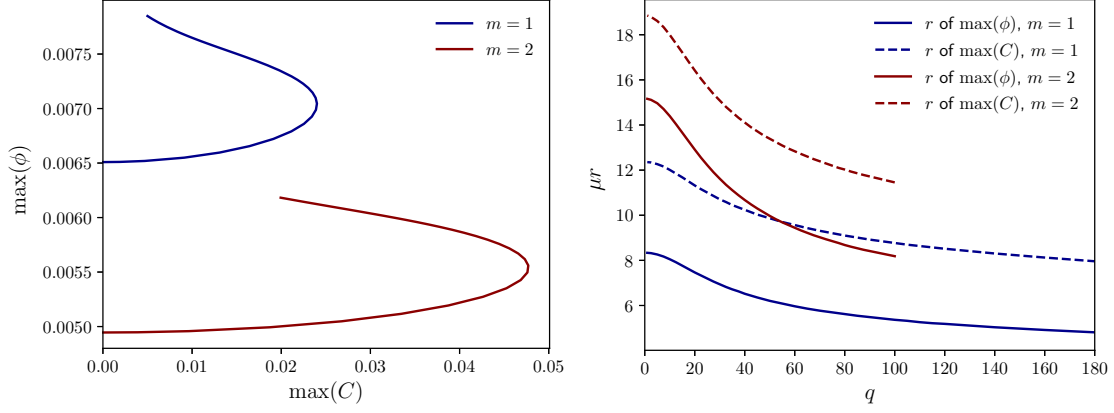


FIG. 5. Sequence of solutions constant ω and increasing coupling q . Given q we locate in the solution for the maximum of ϕ and C and its location. Left panel: Maximum value of the scalar field with respect to the maximum value of the four potential function C for sequence of solutions with $m = 1$ and $m = 2$ with $\omega = 0.96\mu$. Right panel: Radius at which the maxima of ϕ and C is attained, as a function of the coupling constant q .

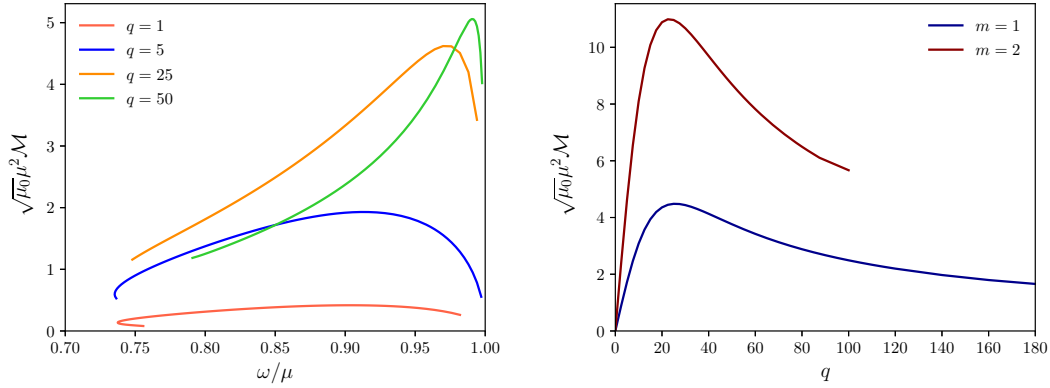


FIG. 6. Left panel: Frequency vs. magnetic dipole moment \mathcal{M} for the $m = 1$ magnetostatic boson star solutions using different values of the coupling constant q . Right panel: Magnetic dipole moment \mathcal{M} as a function of q for configurations with $m = 1$ and $m = 2$ and a fixed value of ω .

property of the solutions: $\max(C)$ reaches a maximum value and then begins to decrease with q . As a consequence, the magnetic dipole moment \mathcal{M} which can be obtained from the asymptotic behavior of the electromagnetic potential A_μ ,

$$A_\mu dx^\mu \sim \frac{\mu_0}{4\pi} \frac{\mathcal{M} \sin^2 \theta}{r} d\varphi, \quad (23)$$

reaches a maximum and decreases thereafter. This behavior is shown in the right panel of Fig. 6 for the sequence of $m = 1$ solutions using four selected values of q and in the same panel can be seen for fixed ω , $m = 1, 2$ and several values of q . One can note from these plots that larger values for the maximum of \mathcal{M} are obtained, closer to $\omega = \mu$, as q increases. In Table I we provide data of the maximum \mathcal{M} configuration for a sample of values for the coupling constant. For the explored $q \gg 1$ configurations, the maximum of \mathcal{M} increases more slowly, for example, the $q = 200$ case, with $\max(\mathcal{M}) = 4.84$, is not far from the value obtained for the $q = 50$ case, plotted in Fig. 6, so the maximum dipole moment seems to tend asymptotically to a finite value, however to establish with precision the limit, it would be necessary to solve the equations in the limiting case $q \rightarrow \infty$, which is beyond the scope of this paper.

Finally, we wonder about the possibility of determining the magnetic dipole moment from the asymptotic behavior of the metric functions. For example, in the charged mini-boson star, the total electric charge of the configuration can be read off the g_{rr} component by comparing with the Reissner-Nordström solution [13]. Some electrovacuum exact solutions (in General Relativity) for a mass endowed with a magnetic dipole moment have been obtained in the literature, as for example the Gutsunaev-Manko [40] and Bonnor [41] two-parameter family of solutions. However, analyzing our solutions, we obtain that they do not match with neither of those metrics, for instance the lapse function in all of the solutions that we generate has the asymptotic behavior $N^2 = 1 - 2M/r + \alpha/r^2 + \mathcal{O}(1/r^3)$, with α some constant, while according to [40], the lapse of the Gutsunaev-Manko metric goes as $N^2 = 1 - 2M/r + \mathcal{O}(1/r^3)$. On

TABLE I. Maximum mass and magnetic dipole configurations.

	q	$\sqrt{\mu_0}\mu^2\mathcal{M}$	ω/μ	μM	$\mu^2\mathcal{N}$	$\max(\phi)$	$\mu r_{\max(\phi)}$
Maximum \mathcal{M}							
	0.1	0.0418	0.905	1.048	1.077	0.0156	4.66
	1	0.417	0.905	1.047	1.076	0.0156	4.66
	5	1.93	0.911	1.015	1.041	0.0147	4.82
	25	4.62	0.970	0.627	0.633	0.00492	9.08
	50	5.06	0.990	0.363	0.363	0.00154	16.8
	100	5.17	0.997	0.195	0.195	0.000454	30.1
	200	4.84	0.999	0.084	0.085	0.000132	36.0
Maximum M							
	0	0	0.840	1.147	1.189	0.0290	2.76
	0.1	0.0368	0.834	1.147	1.189	0.0303	2.65
	1	0.366	0.834	1.146	1.188	0.0303	2.65
	5	1.66	0.839	1.121	1.160	0.0296	2.69
	25	2.46	0.848	0.960	0.989	0.0312	2.22
	50	1.69	0.848	0.894	0.921	0.0337	1.85

the other hand, comparison with the Bonnor solution, for which $N^2 = 1 - 2M/r + M^2/r^2$, could seem to be a better alternative, however we obtain from the analysis of our solutions that the coefficient α is a function of both of M and \mathcal{M} and in the $\mathcal{M} = 0$ case, it is not proportional to M^2 . Therefore the magnetic dipole moment of the star cannot be obtained from the metric components by comparison with any of the mentioned exact solutions, allowing us to conclude that our solutions differ from those two spacetimes.

IV. MAGNETIC FIELD

The electric and magnetic field as measured by an observer whose four-velocity is n^μ (Eulerian observer) are given by the formulas $E_\mu = F_{\mu\nu}n^\nu$ and $B_\mu = -\frac{1}{2}\epsilon_{\mu\nu\alpha\beta}n^\nu F^{\alpha\beta}$, where ϵ is the Levi-Civita tensor. For the metric (8) and the electromagnetic four-potential (10), we obtain $E_\mu = 0$ as expected and

$$B_\mu dx^\mu = \frac{e^{-F_2}}{\sin\theta} \left(\frac{1}{r^2} \frac{\partial C}{\partial\theta} dr - \frac{\partial C}{\partial r} d\theta \right). \quad (24)$$

Some examples of B^i for configurations with $m = 1$ are given in Fig. 7. The distribution of the vector field resemble that of the magnetic field around a finite size current loop. For reference we also plot the isocontour of half the maximum value of the energy density. Rotation of this curve around the z axis generates a torus. The figure also shows the region of zero magnetic field that forms in configurations with high values of q , where $m - qC \approx 0$, see for instance the black line region with $\sqrt{B^i B_i}/(\mu\sqrt{\mu_0}) < 10^{-6}$ inside the torus in the right panel of Fig. 7.

We have seen in the previous section that as q get closer to zero, the magnetic moment decreases and the maximum values of ϕ and C are reached at larger radii. This explains why some of the configurations with relative low values of q , as for example the $q = 5$ and $q = 25$ cases (Fig. 7, left and central panels), do not have the maximum of B^i at the center of the star but in a toroidal region around the center, while other configurations as for instance the $q = 140$ case (Fig. 7, right panel), posses magnetic fields concentrated in a central region with maximum along $\theta = 0$.

Until now it has not been required to specify the value for the mass parameter of the scalar field given that solutions with different μ are related to each other by rescaling rules. In particular, we have used these rules to construct dimensionless quantities (*e.g.*, μr , ω/μ , μM , $B^\mu/(\mu\sqrt{\mu_0})$, etc.), used in the numerical implementation and in the results reported in previous sections. We now proceed to recover units of different physical quantities in order to compare magnetostatic boson stars with magnetized neutron star solutions. Restoring c and G , the dimensionless quantities related to the total mass of the star and the norm of the magnetic field ($B^2 = B^\mu B_\mu$) are $Gc^{-2}\mu M$ and $Gc^{-4}B^2/(\mu^2\mu_0)$. Furthermore, the product

$$\mathcal{I} := \frac{1}{c^4} \sqrt{\frac{G^3}{\mu_0}} MB, \quad (25)$$

is dimensionless and, more importantly, do not rescale with μ . Evaluating the magnetic field at the center of the star we define $\mathcal{I}_c = \mathcal{I}|_{r=0}$ and plot it along $m = 1$ sequences in Fig. 8.

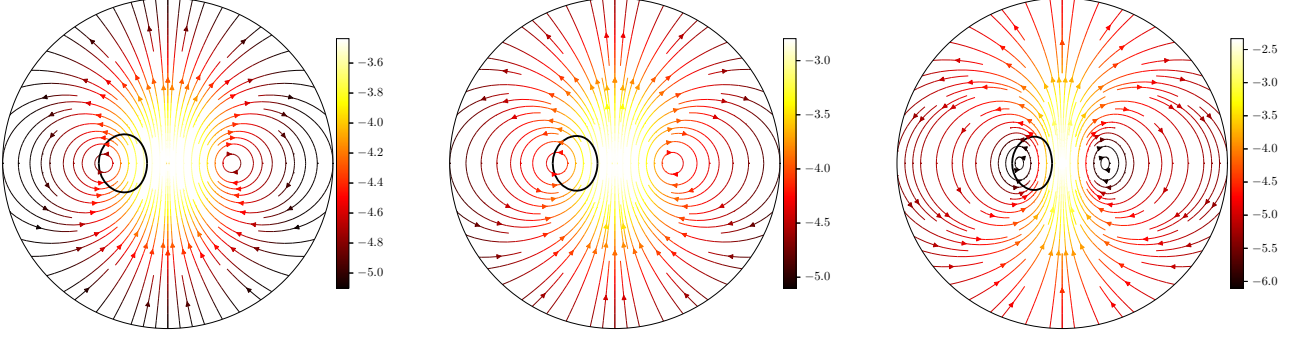


FIG. 7. Magnetic field in a plane of constant φ for configurations with $m = 1$ and $\omega = 0.96\mu$, for the coupling constant with values (from left to right) $q = 5, 25$ and 140 . The thick black line correspond to the density isocountour $E = 0.5 \max(E)$. The color bar indicates the norm of the quantity $\log_{10}[B^i/(\mu\sqrt{\mu_0})]$. The radius of the circle is $\mu r = 32$.

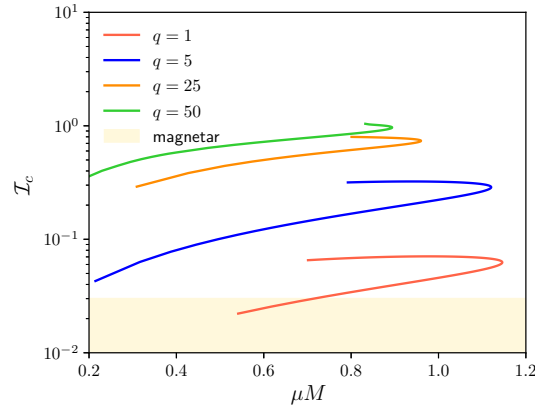


FIG. 8. Dimensionless quantity \mathcal{I} defined in Eq. (25), evaluated at $r = 0$ for configurations with $m = 1$ and different values of q . The yellow region corresponds to the upper region of the interval \mathcal{I} at the center of strongly magnetized neutron stars (see the text for details).

For a neutron star with mass in the range $1.1M_\odot \lesssim M \lesssim 2.1M_\odot$ and strong magnetic fields at the star's pole within the interval $10^9\text{T} \lesssim B_{\text{pole}} \lesssim 10^{11}\text{T}$ [42], the value of the product of mass and magnetic field is between $10^{-7} \lesssim \mathcal{I}_{\text{pole}} \lesssim 3 \times 10^{-5}$. Internal magnetic fields in magnetars have been estimated according to simulations to be as high as³ 10^{14}T . An extended range for \mathcal{I} at the center of strongly magnetized neutron stars would be $10^{-7} \lesssim \mathcal{I}_c \lesssim 3 \times 10^{-2}$.

As can be appreciated from Fig. 8, some of the individual configurations intersect with the interval $10^{-7} \lesssim \mathcal{I}_c \lesssim 3 \times 10^{-2}$, which means that it is possible to find a value of μ such that B_c and M are within the range of neutron stars. In particular some of the low mass solutions obtained with $q = 1$ are in this region, while typical, compact solutions with $q = 1, 5, 25$ and 50 might have stronger magnetic fields (larger masses) than magnetars if we assume similar values of the mass (magnetic fields) of the boson stars to those of the neutron star models. In order to perform a numerical application we restrict to the configurations with $q = 1$ and $M\mu = 0.7$ and choose $M = 1.5M_\odot$. This fixes $\mu(c\hbar) = 1.8 \times 10^{-10}\text{eV}$ which in turn sets the magnitude of all other physical variables, for instance the magnitude of the magnetic field at the center of coordinates takes then the value of $B_c \approx 1 \times 10^{14}\text{T}$, which is within the expected values of magnetic fields inside magnetars. Furthermore, the size of this bosonic configuration, which can be estimated from the size of the torus, is of order $r_{\text{max}(\phi)} \approx 9\text{ km}$, obtaining a compactness comparable to those of neutron stars.

³ Restricting to the Einstein-Maxwell-Euler self-consistent models of neutron stars with equations of state independent of the magnetic field, the maximum magnetic field B_c , which is attained at the center of the star, is approximately only one order of magnitude bigger than B_{pole} (see *e.g.*, [20]).

V. CONCLUSIONS

In the present work we have constructed magnetized solutions of boson stars, which are static, axisymmetric, everywhere regular and asymptotically flat solutions of the Einstein-Maxwell-Klein-Gordon system characterized by the mass parameter of the scalar field μ , the azimuthal harmonic index (winding number) m and the coupling constant q . The configurations consist of two contrarotating oppositely charged tori, and we have seen that they give rise to an electrically neutral current that generates a poloidal magnetic field, according to the observer at rest.

Comparing with the $q = 0$ case, which reduces to the toroidal static boson stars found in [19], we obtained that the electromagnetic field affects the structure of the star and can noticeably change their mass and size. Similarly to other boson star models, in the magnetostatic solutions obtained in this work, a maximum mass configuration was found for each q , and in all explored cases the sequence of solutions contain a region of negative binding energy. Regarding the electromagnetic part, the dipole magnetic moment \mathcal{M} has been obtained and an important difference is noted with respect to the rotating charged boson star, namely that the maximum \mathcal{M} configuration does not corresponds with the maximum mass configuration for every q , and is shifted towards the zero mass solution ($\omega = \mu$).

We showed that regions of zero magnetic field form at the inner part of the torus which grow in size as one considers large enough values of the electromagnetic coupling constant q . On the other hand, it has also been found that the electromagnetic contribution to the sources increases in relation to the scalar field corresponding sources. For these reasons and since we have not found any bound for q , it would be interesting to study in a future work, the numerically challenging solutions with $q \gg 1$ and also analyze the asymptotic limit $q \rightarrow \infty$.

The magnetic field has been compared to that of strongly magnetized neutron stars, obtaining that for similar values of the total mass of the star, the inner magnetic field is comparable to that of magnetars for $q \lesssim 1$ compact configurations and greater, for larger values of q , making our objects, besides being interesting by their own value, faithful mimickers of neutron stars. Since toroidal static boson stars with $q = 0$ are known to be unstable we expect that the obtained solutions (at least for small values of q) remain unstable, however there is a stabilization mechanism for neutral multifield boson stars [19] which might be applied to the charged scalar field case. Boson stars are useful entities in strong gravity research, in particular in dynamical studies and as toy models of more complex scenarios. In this sense, the compactness and magnetic field magnitudes of magnetostatic boson stars motivates the study of the collapse and the consequent emission in both the gravitational and electromagnetic channels. Such collapse dynamics and multimessenger studies will be presented in future works.

ACKNOWLEDGMENTS

We thank Juan Carlos Degollado and Olivier Sarbach for their useful comments in the elaboration of this manuscript. This work was partially supported by DGAPA-UNAM through grants IN110218 and IN105920, by the CONACyT Network Project No. 376127 “Sombras, lentes y ondas gravitatorias generadas por objetos compactos astrofísicos”. VJ acknowledge financial support from CONACyT graduate grant program.

Appendix A: 3+1 decomposition of $T_{\mu\nu}$ and the elliptic system of PDEs

In terms of energy-momentum tensor decomposed into de 3+1 quantities,

$$E = T_{\mu\nu}n^\mu n^\nu; \quad P_\alpha = -n^\nu T_{\mu\nu}\gamma_\alpha^\nu; \quad S_{\alpha\beta} = T_{\mu\nu}\gamma_\alpha^\mu\gamma_\beta^\nu. \quad (\text{A1})$$

where $n^\alpha = (1/N, 0, 0, 0)$, $\gamma_\beta^\alpha = \delta_\beta^\alpha + n^\alpha n_\beta$ and $N := e^{F_0}$, the Einstein equations can be written [27, 43, 44] as the following system of elliptic equations for the metric coefficients at Eq.(8),

$$\Delta_3 F_0 = 4\pi e^{2F_1} (E + S) - \partial F_0 \partial (F_0 + F_2), \quad (\text{A2a})$$

$$\Delta_2 [(Ne^{F_2} - 1) r \sin \theta] = 8\pi Ne^{2F_1+F_2} r \sin \theta (S^r_r + S^\theta_\theta), \quad (\text{A2b})$$

$$\Delta_2 (F_1 + F_0) = 8\pi e^{2F_1} S^\varphi_\varphi - \partial F_0 \partial F_0, \quad (\text{A2c})$$

where,

$$\Delta_3 := \frac{\partial^2}{\partial r^2} + \frac{2}{r} \frac{\partial}{\partial r} + \frac{1}{r^2} \frac{\partial^2}{\partial \theta^2} + \frac{1}{r^2 \tan \theta} \frac{\partial}{\partial \theta}, \quad (\text{A3})$$

$$\Delta_2 := \frac{\partial^2}{\partial r^2} + \frac{1}{r} \frac{\partial}{\partial r} + \frac{1}{r^2} \frac{\partial^2}{\partial \theta^2}, \quad (\text{A4})$$

$$\partial f_1 \partial f_2 := \frac{\partial f_1}{\partial r} \frac{\partial f_2}{\partial r} + \frac{1}{r^2} \frac{\partial f_1}{\partial \theta} \frac{\partial f_2}{\partial \theta}. \quad (\text{A5})$$

The source terms using the ansatz in Eqs. (8), (9) and (10) lead to the following expressions:

$$E + S = \frac{4}{N^2} \omega^2 \phi^2 - 2\mu^2 \phi^2 + \frac{e^{-2(F_1+F_2)}}{\mu_0 r^2 \sin^2 \theta} \partial C \partial C, \quad (\text{A6})$$

$$S^r_r + S^\theta_\theta = 2 \left[\frac{\omega^2}{N^2} - \frac{e^{-2F_2}(m-qC)^2}{r^2 \sin^2 \theta} \right] \phi^2 - 2\mu^2 \phi^2, \quad (\text{A7})$$

$$S^\varphi_\varphi = \left[\frac{\omega^2}{N^2} + \frac{e^{-2F_2}(m-qC)^2}{r^2 \sin^2 \theta} \right] \phi^2 - e^{-2F_1} \partial \phi \partial \phi - \mu^2 \phi^2 + \frac{e^{-2(F_1+F_2)}}{2\mu_0 r^2 \sin^2 \theta} \partial C \partial C. \quad (\text{A8})$$

The two Klein Gordon Eqs., (3), and the Maxwell Eq., (4), reduce to,

$$\Delta_3 \phi = e^{2F_1} \left(\mu^2 - \frac{\omega^2}{N^2} \right) \phi - \partial \phi \partial (F_0 + F_2) + e^{2F_1-2F_2} \frac{(m-qC)^2 \phi}{r^2 \sin^2 \theta}, \quad (\text{A9})$$

$$(2\Delta_2 - \Delta_3)C = -\partial C \partial (F_0 - F_2) - 2\mu_0 q e^{2F_1} (m-qC) \phi^2. \quad (\text{A10})$$

We have obtained the following number density currents,

$$j_1^\mu = \left(\omega \frac{\phi^2}{N^2}, 0, 0, \frac{e^{-2F_2}(m-qC)\phi^2}{r^2 \sin^2 \theta} \right), \quad (\text{A11})$$

and

$$j_2^\mu = \left(\omega \frac{\phi^2}{N^2}, 0, 0, -\frac{e^{-2F_2}(m-qC)\phi^2}{r^2 \sin^2 \theta} \right), \quad (\text{A12})$$

which have been inserted in Eq. (4) to obtain Eq. (A10), and corresponds to the nontrivial remaining Maxwell equation, $\square A^\varphi - R^\varphi_\varphi = -\mu_0 J^\varphi$.

The Eqs. (A2), (A9) and (A10) make up the elliptic system of PDEs for the model (1) using the ansatz presented at section II.

-
- [1] J. C. Bustillo, N. Sanchis-Gual, A. Torres-Forné, J. A. Font, A. Vajpeyi, R. Smith, C. Herdeiro, E. Radu, and S. H. W. Leong, *Phys. Rev. Lett.* **126**, 081101 (2021), [arXiv:2009.05376 \[gr-qc\]](#).
 - [2] F. S. Guzman and J. M. Rueda-Becerril, *Phys. Rev. D* **80**, 084023 (2009), [arXiv:1009.1250 \[astro-ph.HE\]](#).
 - [3] C. A. R. Herdeiro, A. M. Pombo, E. Radu, P. V. P. Cunha, and N. Sanchis-Gual, *JCAP* **04**, 051 (2021), [arXiv:2102.01703 \[gr-qc\]](#).
 - [4] S. Tsujikawa, *Class. Quant. Grav.* **30**, 214003 (2013), [arXiv:1304.1961 \[gr-qc\]](#).
 - [5] A. Suárez, V. H. Robles, and T. Matos, *Astrophys. Space Sci. Proc.* **38**, 107 (2014), [arXiv:1302.0903 \[astro-ph.CO\]](#).
 - [6] L. Hui, J. P. Ostriker, S. Tremaine, and E. Witten, *Phys. Rev. D* **95**, 043541 (2017), [arXiv:1610.08297 \[astro-ph.CO\]](#).
 - [7] L. A. Ureña López, *Front. Astron. Space Sci.* **6**, 47 (2019).
 - [8] A. H. Guth, *Phys. Rev. D* **23**, 347 (1981).
 - [9] S. L. Liebling and C. Palenzuela, *Living Rev. Rel.* **15**, 6 (2012), [arXiv:1202.5809 \[gr-qc\]](#).
 - [10] L. Visinelli, *Int. J. Mod. Phys. D* **30**, 2130006 (2021), [arXiv:2109.05481 \[gr-qc\]](#).
 - [11] Y. Shnir, (2022), [arXiv:2204.06374 \[gr-qc\]](#).
 - [12] D. J. Kaup, *Phys. Rev.* **172**, 1331 (1968).
 - [13] P. Jetzer and J. J. van der Bij, *Phys. Lett. B* **227**, 341 (1989).
 - [14] S. Yoshida and Y. Eriguchi, *Phys. Rev. D* **56**, 762 (1997).
 - [15] L. G. Collodel, B. Kleihaus, and J. Kunz, *Phys. Rev. D* **99**, 104076 (2019), [arXiv:1901.11522 \[gr-qc\]](#).
 - [16] C. A. R. Herdeiro, J. Kunz, I. Perapechka, E. Radu, and Y. Shnir, *Phys. Lett. B* **812**, 136027 (2021), [arXiv:2008.10608 \[gr-qc\]](#).
 - [17] M. Alcubierre, J. Barranco, A. Bernal, J. C. Degollado, A. Diez-Tejedor, M. Megevand, D. Nunez, and O. Sarbach, *Class. Quant. Grav.* **35**, 19LT01 (2018), [arXiv:1805.11488 \[gr-qc\]](#).
 - [18] V. Jaramillo, N. Sanchis-Gual, J. Barranco, A. Bernal, J. C. Degollado, C. Herdeiro, and D. Núñez, *Phys. Rev. D* **101**, 124020 (2020), [arXiv:2004.08459 \[gr-qc\]](#).
 - [19] N. Sanchis-Gual, F. Di Giovanni, C. Herdeiro, E. Radu, and J. A. Font, *Phys. Rev. Lett.* **126**, 241105 (2021), [arXiv:2103.12136 \[gr-qc\]](#).
 - [20] M. Bocquet, S. Bonazzola, E. Gourgoulhon, and J. Novak, *Astron. Astrophys.* **301**, 757 (1995), [arXiv:gr-qc/9503044](#).
 - [21] C. Y. Cardall, M. Prakash, and J. M. Lattimer, *Astrophys. J.* **554**, 322 (2001), [arXiv:astro-ph/0011148](#).
 - [22] D. Chatterjee, T. Elghozi, J. Novak, and M. Oertel, *Mon. Not. Roy. Astron. Soc.* **447**, 3785 (2015), [arXiv:1410.6332 \[astro-ph.HE\]](#).
 - [23] A. Oron, *Phys. Rev. D* **66**, 023006 (2002).

- [24] K. Kiuchi and S. Yoshida, *Phys. Rev. D* **78**, 044045 (2008), [arXiv:0802.2983 \[astro-ph\]](#).
- [25] J. Frieben and L. Rezzolla, *Mon. Not. Roy. Astron. Soc.* **427**, 3406 (2012), [arXiv:1207.4035 \[gr-qc\]](#).
- [26] S. W. Hawking and G. F. R. Ellis, *The Large Scale Structure of Space-Time*, Cambridge Monographs on Mathematical Physics (Cambridge University Press, 2011).
- [27] P. Grandclement, C. Somé, and E.ourgoulhon, *Phys. Rev. D* **90**, 024068 (2014), [arXiv:1405.4837 \[gr-qc\]](#).
- [28] S. Ontanon and M. Alcubierre, *Class. Quant. Grav.* **38**, 154003 (2021), [arXiv:2103.13993 \[gr-qc\]](#).
- [29] H. Stephani, D. Kramer, M. A. H. MacCallum, C. Hoenselaers, and E. Herlt, *Exact solutions of Einstein's field equations*, Cambridge Monographs on Mathematical Physics (Cambridge Univ. Press, Cambridge, 2003).
- [30] E.ourgoulhon, in *CompStar 2010: School and Workshop on Computational Tools for Compact Star Astrophysics* (2010) [arXiv:1003.5015 \[gr-qc\]](#).
- [31] C. A. R. Herdeiro, J. Kunz, I. Perapechka, E. Radu, and Y. Shnir, *Phys. Rev. D* **103**, 065009 (2021), [arXiv:2101.06442 \[gr-qc\]](#).
- [32] P. Grandclement, *J. Comput. Phys.* **229**, 3334 (2010), [arXiv:0909.1228 \[gr-qc\]](#).
- [33] P. Grandclement, “Kadath library,” (2009).
- [34] P. Grandclement and J. Novak, *Living Rev. Rel.* **12**, 1 (2009), [arXiv:0706.2286 \[gr-qc\]](#).
- [35] M. Alcubierre, J. Barranco, A. Bernal, J. C. Degollado, A. Diez-Tejedor, V. Jaramillo, M. Megevand, D. Núñez, and O. Sarbach, *Class. Quant. Grav.* **39**, 094001 (2022), [arXiv:2112.04529 \[gr-qc\]](#).
- [36] G. Quintero Angulo, A. Pérez Martínez, H. Pérez Rojas, and D. Manreza Paret, *Int. J. Mod. Phys. D* **28**, 1950135 (2019), [arXiv:1812.07657 \[astro-ph.HE\]](#).
- [37] D. Pugliese, H. Quevedo, J. A. Rueda H., and R. Ruffini, *Phys. Rev. D* **88**, 024053 (2013), [arXiv:1305.4241 \[astro-ph.HE\]](#).
- [38] G. Raposo, P. Pani, M. Bezares, C. Palenzuela, and V. Cardoso, *Phys. Rev. D* **99**, 104072 (2019), [arXiv:1811.07917 \[gr-qc\]](#).
- [39] H. Andreasson, *J. Diff. Eq.* **245**, 2243 (2008), [arXiv:gr-qc/0702137](#).
- [40] T. Gutsunaev and V. Manko, *Physics Letters A* **123**, 215 (1987).
- [41] W. B. Bonnor, *Zeitschrift für Physik* **190**, 444 (1966).
- [42] V. M. Kaspi and A. Beloborodov, *Ann. Rev. Astron. Astrophys.* **55**, 261 (2017), [arXiv:1703.00068 \[astro-ph.HE\]](#).
- [43] S. Bonazzola, E.ourgoulhon, M. Salgado, and J. A. Marck, *Astron. Astrophys.* **278**, 421 (1993).
- [44] E.ourgoulhon, P. Haensel, R. Livine, E. Paluch, S. Bonazzola, and J. A. Marck, *Astron. Astrophys.* **349**, 851 (1999), [arXiv:astro-ph/9907225](#).